

Chaotic Fields Behave Universally Out of Equilibrium

D. Lippolis¹

School of Mathematical Sciences, Jiangsu University, 212013 Zhenjiang, China.

(*Electronic mail: domenico@ujs.edu.cn)

(Dated: 4 June 2024)

Chaotic dynamics is always characterized by swarms of unstable trajectories, unpredictable individually, and thus generally studied statistically. It is often the case that such phase-space densities relax exponentially fast to a limiting distribution, that rules the long-time average of every observable of interest. Before that asymptotic time scale, the statistics of chaos is generally believed to depend on both the initial conditions and the chosen observable. I show that this is not the case for a widely applicable class of models, that feature a phase-space distribution common to all pushed-forward or integrated observables, while the system is still relaxing towards statistical equilibrium or a stationary state. This universal profile is determined by both leading and first subleading eigenfunctions of the transport operator (Koopman or Perron-Frobenius) that maps phase-space densities forward or backward in time.

Chaotic processes are ever present in nature, and they typically reach a statistically-equilibrated- or a stationary state, that determines the distributions of trajectories and long-time averages of relevant observables, such as diffusivity, energy or instability. These limiting distributions are the leading eigenfunctions of a linear operator (Koopman or Perron-Frobenius) that transports densities in the phase space. At intermediate time scales, the system is still relaxing and the expectation values depend on the initial conditions. Yet, the finite-time, phase-space distributions of *all* observables are shown here to follow a combination of the first two eigenfunctions of the transport operator. That enables us to predict the density profile of any quantity of interest by only computing the first two eigenfunctions of the density-transport operator spectrum.

I. INTRODUCTION

As a fact of nature, chaos is unpredictable, due to the extreme sensitivity of trajectories to initial conditions, and the finite precision of our computers. Impossible as it is to solve the problem of motion, practitioners resort to the tools of statistical mechanics to estimate averages and fluctuations of observables of interest (energy, diffusion constant, Lyapunov exponents, vorticity, etc.). That feat is achievable for long-time evolution, provided that the system in exam be ergodic, and that it asymptotically relax to a limiting distribution usually called natural measure, the weight function of phase-space averages.

The natural measure (or invariant density) is the leading eigenfunction of the Perron-Frobenius transport operator \mathcal{L}_t ,¹ that evolves densities in time throughout the phase space, and whose leading eigenvalue determines the escape rate. As the resolvent to the Liouville equation, this operator is linear, but infinite dimensional². Especially in the Koopman form (adjoint of Perron-Frobenius), transport operators have found countless applications in recent years³⁻⁷, thanks to the genericity of the Markov property throughout modelling⁸, and so have their finite-dimensional discretizations⁹⁻¹¹, which lend themselves to a faster time-iteration and a practical spectral

analysis.

Spectrum wise, the first subleading eigenvalue yields information on the speed of relaxation of the system to statistical equilibrium or a stationary state, and on the typical time scale of the decay of correlations. In one-dimensional chaos, the second eigenvalue of the Perron-Frobenius operator has been related to the Lyapunov exponent of the dynamics¹². Still, the role of the corresponding eigenfunction was little investigated¹³ until recently, when in strong chaos^{14,15} and two-dimensional vector fields¹⁶, it was shown to exhibit similar patterns as the field of local instabilities in the phase space, that is the finite-time Lyapunov exponents.

The present report extends these findings by demonstrating that the first two eigenfunctions of the transfer operator spectrum govern not only the phase-space profiles of the finite-time Lyapunov exponents, but also those of *any* field derived from numerically integrated trajectories ('Lagrangian' point of view in fluid dynamics), that is the phase-space distribution¹⁷ of an observable mapped forward (or backward) in time, before relaxation to equilibrium or a stationary state.

The formal analysis revolves around time-dependent dynamical averages, initially defined to compute expectation values, but successively transformed to full distributions in the phase space, more informative than single statistical moments that depend on initial conditions. Next, the time evolution of the phase-space densities that serve as weight functions for the dynamical averages is expanded in terms of the eigenfunctions the transfer operator. That connects the observables to the leading and subleading eigenfunctions of the spectrum, the central result of this work. The observable independent and thus universal behavior of the field profiles stems from their connection to these eigenfunctions, and it also extends to the so-called time-integrated observables, such as finite-time Lyapunov exponents, or diffusion constants. Moreover, the derived formalism and results apply to chaotic systems with weak noise, besides purely deterministic ones. Numerical tests are run on two representative models of chaotic dynamics, namely the perturbed cat map, and the Hamiltonian Hénon map, in order to validate theory and universality claims.

II. TIME-DEPENDENT STATISTICS OF CHAOTIC OBSERVABLES

A. Mapping phase-space averages

Given an observable $a(x)$ defined as a function or an operator in the phase space \mathcal{M} , its expectation value may be written as

$$\langle a \rangle = \frac{1}{\mu_{\mathcal{M}}(\rho)} \int_{\mathcal{M}} a(x) \rho(x) dx, \quad (1)$$

where $\rho(x)$ is the phase space density, that is the frequency with which trajectories visit \mathcal{M} , while $\mu_{\mathcal{M}}(\cdot)$ is the Lebesgue measure over \mathcal{M} . Both a and ρ are functions of the dynamical variable x , that is advected by a flow $f^t(x)$ as time proceeds. As a result, the expectation value (1) itself depends on time as

$$\langle a^t \rangle = \frac{1}{\mu_{\mathcal{M}}(\rho^t)} \int_{\mathcal{M}} a(f^t(x)) \rho(x) dx. \quad (2)$$

The pushed-forward ('downstream') observable $a(f^t(x))$ may also be expressed through the action of the Koopman operator, $[\mathcal{L}_t^\dagger a](x) = a(f^t(x))$, which is *linear* and rewrites the integral in Eq. (2) as

$$\begin{aligned} \int_{\mathcal{M}} [\mathcal{L}_t^\dagger a](x) \rho(x) dx &= \int_{\mathcal{M}} a(x) [\mathcal{L}_t \rho](x) dx = \\ &= \int_{\mathcal{M}} dx a(x) \int_{\mathcal{M}} dx_0 \delta(x - f^t(x_0)) \rho(x_0), \end{aligned} \quad (3)$$

meaning that one can shift the action of the push-forward operator \mathcal{L}_t^\dagger from the field a to the density ρ , that is instead pulled back by the adjoint \mathcal{L}_t of the Koopman operator, called Perron-Frobenius operator.

B. Chaos and spectral expansions

The Perron-Frobenius operator \mathcal{L}_t is a formal solution to the Liouville equation $\partial_t \rho + \nabla \cdot (\rho v) = 0$, where $\dot{x} = v(x)$ is the dynamical system generating the flow $f^t(x)$. In chaotic systems with no escape and with a proper choice of function space¹⁸, the Perron-Frobenius spectrum has an isolated, unitary eigenvalue, whose ('leading') eigenfunction is called natural measure or invariant density¹⁹. The natural measure is the weight to every phase-space average, and, as such, its successful determination enables us to evaluate any long-term averaged observable under the ergodicity assumption. For an open system, the leading eigenvalue is subunitary and its logarithm is the escape rate²⁰, whereas the associate eigenfunction is called conditionally invariant density. The dynamics of interest here is chaotic, so that one can choose a basis function set and a support for \mathcal{L}_t such that the resulting eigenspectrum be discrete away from the origin of the complex plane²¹. If the system at hand is both chaotic and mixing, time-correlations decay exponentially fast, the near-origin continuous spectrum (within the 'essential radius') is negligible, whereas the sub-leading part of the spectrum of \mathcal{L}_t is discrete and subunitary²:

in particular, the second eigenvalue yields the decay rate of an initial density to the natural measure, and it concerns an intermediate timescale, where the system is still in the process of relaxation towards either statistical equilibrium or a stationary state.

The meaning and avail of the second eigenfunction is the object of the present study, and it is revealed by expanding the piece $[\mathcal{L}_t \rho](x)$ in Eq. (3) in terms of the eigenspectrum of \mathcal{L}_t :

$$\int_{\mathcal{M}} a(x) [\mathcal{L}_t \rho](x) dx = \sum_j b_j e^{-\gamma_j t} \int_{\mathcal{M}} a(x) \phi_j(x) dx \quad (4)$$

is still the numerator of the pushed-forward average $\langle a^t \rangle$ in Eq. (2), that depends on time and initial conditions, and thus it is not so meaningful before the system has reached statistical equilibrium. For that reason, it is sensible to go beyond the single moments and work out an expression for the full phase-space ('field') distribution of a^t that involves the spectrum of \mathcal{L}_t , which, importantly, does not depend on the observable chosen. Such feat can be achieved by first identifying the initial conditions in Eq. (4) with the coefficients

$$b_j = \int_{\mathcal{M}} \rho(x) \phi_j(x) dx, \quad (5)$$

where the $\phi_j(x)$ are eigenfunctions of the Koopman operator \mathcal{L}_t^\dagger (note the difference with the eigenfunctions $\phi_j(x)$ of \mathcal{L}_t), and then by setting the initial density to $\rho(x) = \delta(x - x_0)$, that is entirely concentrated in one point.

That done, the expectation value (2) becomes the function

$$\hat{a}^t(x_0) := \frac{a(f^t(x_0))}{\mu_{\mathcal{M}}(\rho^t)} = \frac{1}{\mu_{\mathcal{M}}(\rho^t)} \sum_j \phi_j(x_0) e^{-\gamma_j t} \int_{\mathcal{M}} a(x) \phi_j(x) dx. \quad (6)$$

The previous expansion will be truncated to the first two terms when considering an intermediate time scale, determined by the spectral gap, as $(\gamma_1 - \gamma_0)^{-1}$. On the other hand, the denominator $\mu_{\mathcal{M}}(\rho^t) = \int dx [\mathcal{L}_t \rho](x)$ is approximated with the first term in the same expansion, so as to obtain, overall,

$$\hat{a}^t(x_0) \simeq \int_{\mathcal{M}} a(x) \phi_0(x) dx + \frac{\phi_1(x_0)}{\phi_0(x_0)} e^{-(\gamma_1 - \gamma_0)t} \int_{\mathcal{M}} a(x) \phi_1(x) dx, \quad (7)$$

where the first term is the long-time average weighed by the natural measure $\phi_0(x)$ (assumed normalized), while the second term characterizes the *profile* of the field $\hat{a}^t(x_0)$ by the ratio of the second to the first eigenfunctions of the Koopman operator \mathcal{L}_t^\dagger , that is *observable independent*. If the system is closed, the escape rate vanishes and thus $\gamma_0 = 0$, while the measure $\mu_{\mathcal{M}}(\rho^t)$ of the density is time independent and may be normalized to unity. That simplifies the approximation (7), that now solely depends on the second eigenfunction $\phi_1(x_0)$ of the Koopman operator for any observable.

If, instead of pushing the observable forward as $[\mathcal{L}_t^\dagger a](x) = a(f^t(x))$, we pull it back ('upstream') by means of the Perron-Frobenius operator, $[\mathcal{L}_t a](x)$, the above derivation still holds under the same assumptions, but the field $\langle a^{-t} \rangle(x_0)$ now depends on the first two eigenfunctions of the

Perron-Frobenius operator \mathcal{L}_t as

$$\hat{a}^{-t}(x_0) := \frac{a(f^{-t}(x_0))}{\mu_{\mathcal{M}}(\rho^t)|J^t(f^{-t}(x_0))|} \simeq \int_{\mathcal{M}} a(x)\varphi_0(x)dx + \frac{\phi_1(x_0)}{\phi_0(x_0)}e^{-(\gamma_1-\gamma_0)t} \int_{\mathcal{M}} a(x)\varphi_1(x)dx, \quad (8)$$

assuming $\varphi_0(x)$ as normalized. Here $J^t(x)$ denotes the Jacobian matrix of the trajectory originating at x and running for time t (definition below), which pops up from the direct application $[\mathcal{L}_t a]$ of the Perron-Frobenius operator to the observable.

The universality in the profiles of the finite-time fields stems from the first-order truncation of a spectral expansion, which leads to Eqs. (7) and (8). The timescale of validity of such approximation, and in particular the relative magnitudes of the second vs. third (neglected) term in the expansions are discussed in Appendix A.

C. Integrated observables

Of special interest in dynamics are the integrated observables², related to Lagrangian averages²² or finite-time Birkhoff averages (by adding a factor of $1/t$):

$$A^t(x) = \int_0^t a[f^\tau(x)] d\tau, \quad (9)$$

where the integral is time ordered, that is, taken along the trajectory $f^t(x)$. The computation of $A^t(x)$ is straightforward if the observable $a(x)$ is a functional field, for example in the phase-space diffusivity

$$D^t(x) = \int_0^t [f^\tau(x) - x]^2 d\tau, \quad (10)$$

but more involved if $a(x)$ is an operator, as it is the case for the Jacobian

$$J^t(x_0) = e^{\int_0^t d\tau M(f^\tau(x_0))}, \quad M_{ij}(x) = \frac{\partial v_i(x)}{\partial x_j}, \quad (11)$$

where the exponential is the formal solution to the matrix differential equation $\frac{dJ^t}{dx} = MJ$ (sometimes called variational initial-value problem²³) along the orbit $x_0 \rightarrow f^t(x_0)$. The quantity of interest is then the stability (or finite-time Lyapunov) exponent $A^t(x_0) = \ln||J^t(x_0)||/t$.

The expectation value (2) can now be generalized to an integrated observable $A^t(x)$ by either *i*) choosing the mapped $[\mathcal{L}_t \rho](x)$ as weight function

$$\langle A^t \rangle_{\rho^t} = \int_{\mathcal{M}} A^t(x) [\mathcal{L}_t \rho](x) dx, \quad (12)$$

which leads to the approximate field distribution pinned at the

initial point of the trajectory $x_0 \rightarrow f^t(x_0)$:

$$\hat{A}^t(x_0) := \frac{A^t(x_0)}{\mu_{\mathcal{M}}(\rho^t)} \simeq \int_{\mathcal{M}} A^t(x)\phi_0(x)dx + \frac{\phi_1(x_0)}{\phi_0(x_0)}e^{-(\gamma_1-\gamma_0)t} \int_{\mathcal{M}} A^t(x)\phi_1(x)dx, \quad (13)$$

or *ii*) by choosing the initial $\rho(x)$ as weight function

$$\langle A^t \rangle_{\rho} = \int_{\mathcal{M}} A^t(x)\rho(x)dx, \quad (14)$$

that results in the observable field pinned at the arrival point of the trajectory $f^{-t}(x_0) \rightarrow x_0$:

$$\hat{A}^{-t}(x_0) := \frac{A(f^{-t}(x_0))}{\mu_{\mathcal{M}}(\rho^t)|J^t(f^{-t}(x_0))|} \simeq \int_{\mathcal{M}} A^t(x)\varphi_0(x)dx + \frac{\phi_1(x_0)}{\phi_0(x_0)}e^{-(\gamma_1-\gamma_0)t} \int_{\mathcal{M}} A^t(x)\varphi_1(x)dx. \quad (15)$$

A full account of time-forward and backward integrated observables for chaotic relaxation processes has been given elsewhere²⁴. Here, it should be remarked that in both expressions (13) and (15) the time-dependence of the integrals $\int_{\mathcal{M}} A^t(x)\varphi_i(x)$ (or $\int_{\mathcal{M}} A^t(x)\phi_i(x)$ backward) can be written explicitly, if the observable $a(x)$ is a simple function of the phase-space coordinates. In that case (see Appendix A for details), the expression for a forward integrated observable (13) (and likewise the backward integration (15)) becomes

$$\hat{A}^t(x_0) \simeq \frac{1-e^{-\gamma_0 t}}{\gamma_0} \int_{\mathcal{M}} a(x)\phi_0(x)dx + e^{-(\gamma_1-\gamma_0)t} \frac{1-e^{-\gamma_1 t}}{\gamma_1} \frac{\phi_1(x_0)}{\phi_0(x_0)} \int_{\mathcal{M}} a(x)\phi_1(x)dx, \quad (16)$$

which produces a non-monotonic decay for the second term, and a longer relaxation time to equilibrium or stationarity than for instantaneous observables. This aspect will also be featured in the numerical analysis of section III.

D. Noise

The above analysis and predictions may be generalized to chaotic systems subject to weak noise, so that the equations of motion take the Langevin form $\dot{x} = v(x) + \eta(t)$, with the time-uncorrelated and Gaussian-distributed random force $\eta(t)$. The transfer operator \mathcal{L}_t (\mathcal{L}_t^\dagger), that is the formal solution to the associate Fokker-Planck equation²⁵, features a noisy kernel, for instance²⁶

$$\mathcal{L}_{\Delta,t} \rho(x) = \frac{1}{\sqrt{4\pi\Delta t}} \int_{\mathcal{M}} dx e^{-(y-f^t(x))^2/4\Delta t} \rho(x), \quad (17)$$

for isotropic noise of amplitude 2Δ . The operator $\mathcal{L}_{\Delta,t}$ and its adjoint can be applied to a density ρ as above, or to an observable a , to obtain its noisy evolution, whereas the integrated observable (9) takes the form

$$A_{\Delta}^t(x) = \int_0^t [\mathcal{L}_{\Delta,\tau}^\dagger a](x) d\tau. \quad (18)$$

III. NUMERICAL VALIDATION

The above predictions are now tested with two different models of chaos, the perturbed cat map and the Hamiltonian Hénon map. The strategy is that to numerically compute the first two eigenfunctions of the Perron-Frobenius and of the Koopman spectrum, and compare their ratio with the distributions of different pushed-forward, pulled-back, or integrated observables for finite time.

First, the transfer operator is discretized by means of Ulam's method²⁷⁻²⁹, that is by subdividing the phase space into N intervals \mathcal{M}_i of equal area, and evaluating the transition probabilities from \mathcal{M}_i to \mathcal{M}_j :

$$[\mathbf{L}_t]_{ij} = \frac{\mu(\mathcal{M}_i \cap f^t(\mathcal{M}_j))}{\mu(\mathcal{M}_i)} \quad (19)$$

with $t = 1$. The numerator of the transition rate (19) is estimated with a Monte Carlo method³⁰, that consists of iterating random initial conditions from each cell \mathcal{M}_i and counting which fraction lands in each \mathcal{M}_j .

The finite-dimensional approximation \mathbf{L}_t obtained with the Ulam method leverages the Markov property of the systems of our interest, but it is in general unstable and must be used with caution¹³. Still, for certain everywhere unstable ('hyperbolic') maps, it was found to well reproduce the leading- and first subleading eigenfunctions of the Perron-Frobenius operator on a space of characteristic functions supported on the intervals \mathcal{M}_i at sufficiently large N ^{14,15}.

A. Perturbed cat map

It is defined by $f(x) = T_\varepsilon \circ T[x]$, with $x = (q, p)$,

$$T \begin{pmatrix} q \\ p \end{pmatrix} = \begin{pmatrix} 1 & 1 \\ 1 & 2 \end{pmatrix} \begin{pmatrix} q \\ p \end{pmatrix} \text{ mod } 1, \quad (20)$$

and

$$T_\varepsilon \begin{pmatrix} q \\ p \end{pmatrix} = \begin{pmatrix} q - \varepsilon \sin 2\pi p \\ p \end{pmatrix} \text{ mod } 1, \quad (21)$$

with $\varepsilon = 0.1$ throughout the simulations. This system is strongly chaotic and hyperbolic, that is, correlations decay exponentially fast with time³¹. It possesses an infinite number of unstable periodic orbits, and, specifically, a fixed point at the origin. The phase space is a 2-torus, there is no escape, and areas are preserved by the time evolution, so that the determinant of the Jacobian matrix of every trajectory is equal to unity, and the first eigenfunction of both the Perron-Frobenius and the Koopman operators is a uniform distribution. Thus, according to Eqs. (7) and (8), the out-of-equilibrium field profile of any pushed-forward, pulled-back or integrated observable is characterized by the second eigenfunction alone.

Fig. 1 shows the numerically computed second eigenfunctions of the Perron-Frobenius and Koopman operators with the Ulam discretization. They are striated along the unstable and stable manifolds respectively, that emanate from the fixed point at the origin.

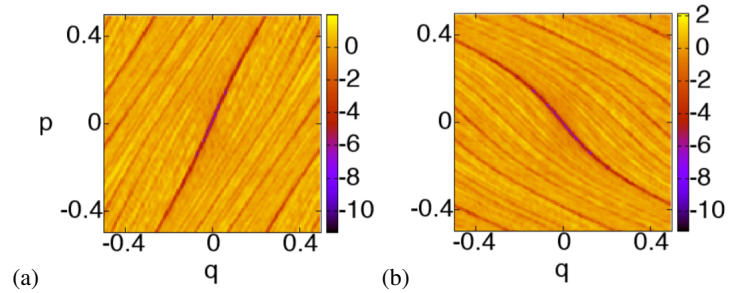


FIG. 1. First subleading eigenfunctions of the (a) Perron-Frobenius and (b) Koopman operator for the perturbed cat map. The Ulam matrix has size $2^{14} \times 2^{14}$.

On the other hand, Figs. 2-3 illustrate the behavior of the numerically computed finite-time fields of three distinct observables, namely the stability (Lyapunov) exponent stemming from the Jacobian (11), the time-integrated kinetic energy $\bar{K}^t(x) = \frac{1}{2} \int_0^t d\tau p^2(f^\tau(x))$, and the instantaneous observables $q^2(x)$ and $p^2(x)$, which are both pushed forward as $q^2(f^t(x))$ or $p^2(f^t(x))$, and pulled back as $q^2(f^{-t}(x))$ or $p^2(f^{-t}(x))$. The fields portrayed in the figures are obtained by iterating some 10^8 randomly chosen, uniformly distributed initial conditions until a certain time t before relaxation. Distinct instantaneous and integrated observables exhibit nearly identical profiles, within the timescales considered. In particular, all finite-time phase space distributions share the features of the second eigenfunction of the Koopman operator (Fig. 1(b)) when pushed forward or pinned by the initial points $x_0 \rightarrow f^t(x_0)$ (Fig. 2(a)-(e)), as predicted by Eqs. (7) and (13). Similarly, they both follow the behavior of the second eigenfunction of the Perron-Frobenius operator (Fig. 1(a)) when pinned by the final point of the same trajectory (Fig. 3(a)-(e)), as expected from Eqs. (8) and (15).

In addition, the logarithmic ratio

$$r(x_0, t) = \ln \left| \frac{\hat{a}_1^t(x_0) - \langle a_1 \rangle_{\mathcal{M}}}{\hat{a}_2^t(x_0) - \langle a_2 \rangle_{\mathcal{M}}} \right|, \quad (22)$$

with $\langle a \rangle_{\mathcal{M}} = \int_{\mathcal{M}} a(x) \phi_0(x) dx$, is reported in Figs. 2-3(c)(f), in order to compare the profiles of any two observables $\hat{a}_1^t(x_0)$ and $\hat{a}_2^t(x_0)$, and quantify their differences as the deviation of Eq. (22) from uniformity. The density plots in the figure indeed suggest that $r(x_0, t)$ is uniform save random fluctuations, which supports the claim of universality of the fields profiles compared.

It is important to observe that significantly shorter iteration times were chosen for the instantaneous ($t \sim 7$) than for the integrated ($t \sim 15$) observables, since the former relax to equilibrium faster (and monotonically) than the latter, as discussed in Appendix A.

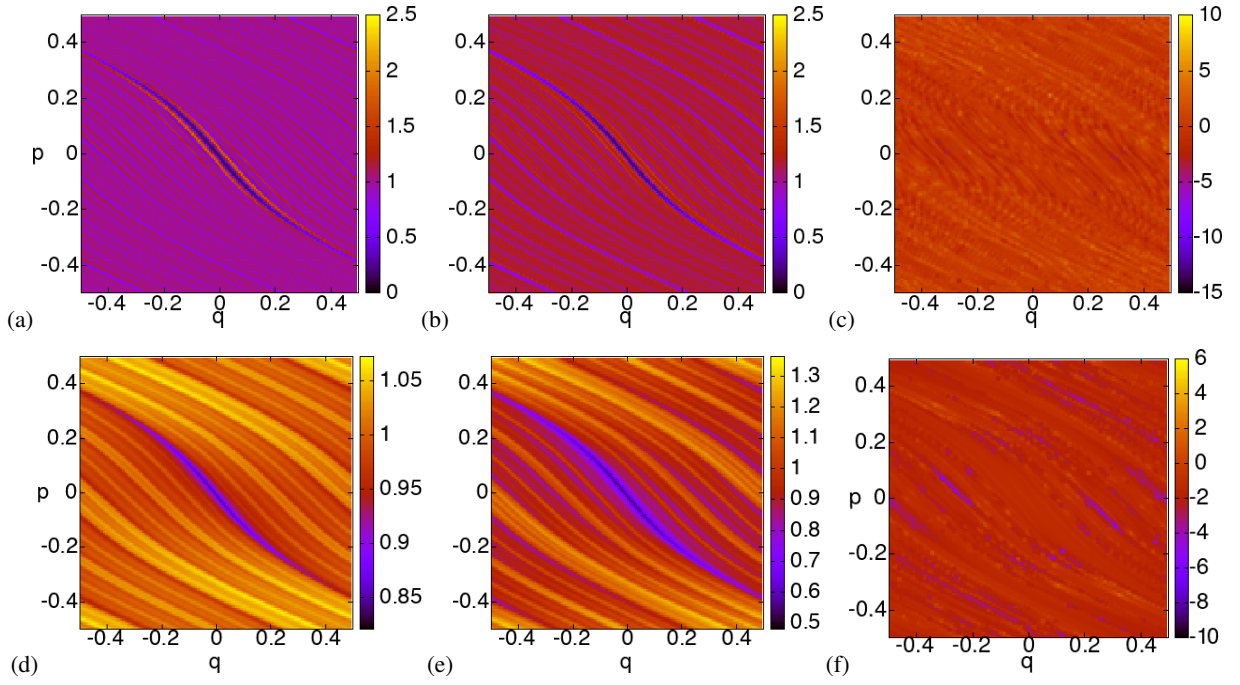


FIG. 2. Perturbed cat map: phase-space density plots (2^{14} points, each averaged over 10^4 trajectories) of (a) the instantaneous kinetic energy $\frac{1}{2}p^2(f^t(x))$ ($t=6$) vs. (b) the observable $q^2(f^t(x))$ ($t=7$), and (c) the logarithmic ratio (22) between the two. (d) The finite-time Lyapunov exponents ($t=15$), and (e) the integrated kinetic energy ($t=15$), versus $x = (q, p)$, initial point of the trajectory $x \rightarrow f^t(x)$. (f) The logarithmic ratio (22) between the two.

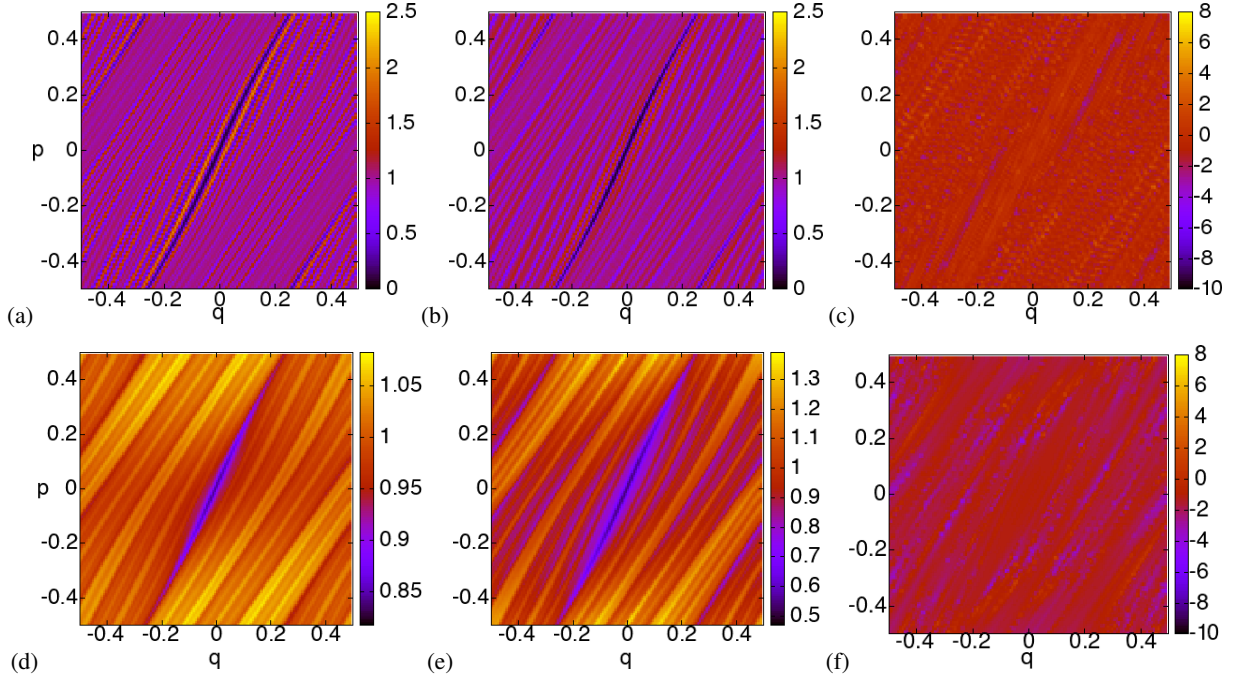


FIG. 3. Perturbed cat map: phase-space density plots (2^{14} points, each averaged over 10^4 trajectories) of (a) the instantaneous kinetic energy $\frac{1}{2}p^2(f^{-t}(x))$ ($t=6$) vs. (b) the observable $q^2(f^{-t}(x))$ ($t=6$), and (c) the logarithmic ratio (22) between the two. (d) The finite-time Lyapunov exponents ($t=15$), and (e) the integrated kinetic energy ($t=15$), versus $x = (q, p)$, final point of the trajectory $f^{-t}(x) \rightarrow x$. (f) The logarithmic ratio (22) between the two.

B. Hamiltonian Hénon map with noise

The next model to test the theory on is the Hamiltonian Hénon map

$$f \begin{pmatrix} q \\ p \end{pmatrix} = \begin{pmatrix} 1 - \alpha q^2 + \beta p \\ q \end{pmatrix} \quad (23)$$

with $\alpha = 1.4$ and $\beta = -1$. This map has no dissipation, but it does allow escape to infinity from the neighborhood of the two

fixed points: $x_p \simeq (-1.1, -1.89)$ is unstable ('hyperbolic') and generates a chaotic saddle through its stable and unstable manifolds, while $x_c \simeq (0.39, 0.39)$ is marginally stable ('center'), and surrounded by a tiny stability island. In order to 'kick' the dynamics out of the latter non-chaotic region and into the chaotic phase, weak noise is added to the map (23) of an amplitude comparable to the size of the stability island per unit time. Strictly speaking, the non-hyperbolicity of the resulting noisy system should introduce a continuous component in the spectrum of the transport operators and thus break the assumption of a solely discrete spectrum. However, if we investigate timescales of the order of- or shorter than the inverse escape rate from the chaotic saddle, when the discrete part of the spectrum is dominant, the contribution of the continuous part of the spectrum may be ignored, due to the smallness of the stability island. Because the system admits escape and the first eigenfunction ϕ_0 (ϕ_0) of \mathcal{L}_t (\mathcal{L}_t^\dagger) is non-uniform, the pushed-forward, pulled-back or integrated observables for intermediate time scales are expected to depend on the ratio of the second to the first eigenfunction of the evolution operator, the latter being non-uniform.

The predictions (13) and (15) are tested for two observables, that is the finite-time Lyapunov exponent and the diffusivity $\hat{D}^t(x) = \int_0^t d\tau [q^2(f^\tau(x)) + p^2(f^\tau(x))]$. The density plots in Fig. 4(a)(b) corroborate the expectations for the fields of the two integrated observables to be supported on the stable manifold of the map when pinned by the initial points of the iteration $x_0 \rightarrow f^t(x_0)$ plus weak noise, and to mimic the density profile of the ratio between the second and the first eigenfunction of the Koopman operator (Fig. 4(f)). The two distinct fields in Fig. 4(a)(b) display almost indistinguishable profiles, as once again confirmed by the near-uniform pattern of their ratio, Eq. (22), Fig. 4(c).

Analogously, the same two observables pinned by the final points of each phase-space trajectory $f^{-t}(x_0) \rightarrow x_0$ plus weak noise produce fields supported on the unstable manifold of the map (Fig. 5(a)(b)). Lyapunov exponent and diffusivity exhibit twin profiles (see their ratio in (Fig. 5(f))), and behave similarly to the ratio of the second to the first eigenfunction of the Perron-Frobenius operator (Fig. 5(e)).

In both 'forward' and 'backward' pictures, the strongly chaotic phase (in orange) is distinguishable from the non-hyperbolic, weakly chaotic phase (in blue) of a three-lobed shape with tapered ends, due to a period-three unstable periodic orbit that rules the dynamics just outside the stability island.

The white color in Figs. 4-5(a)(b) represents the region of the phase space where forward (Fig. 4) or backward (Fig. 5) trajectories escape from the domain examined before the time t of integration, and thus it is not part of the field distributions. In Figs. 4(f) and 5(e), instead, the ratio between the eigenfunctions is not defined in the blank region, where the leading eigenfunction vanishes. The density plots of the leading- and subleading eigenfunctions of the transport operators (Figs. 4(d)(e) and 5(c)(d)) taken separately, bear significant differences from the fields of the observables: the first eigenfunctions clearly describe a longer timescale than that of the fields, at which noisy trajectories have mostly escaped the

hyperbolic region, while they only survive in and around the stability island; the second eigenfunctions alone are more reminiscent of the finite-time fields, except they are suppressed on a ring around the stability island, a feature that does not appear in the density plots of the observables. That supports the necessity of computing the ratio between the eigenfunctions to reproduce the field profiles.

IV. DISCUSSION

Time-dependent observables advected in the phase space by a chaotic dynamical system and before relaxation to statistical equilibrium exhibit universal features, determined by the first two eigenfunctions of the Perron-Frobenius or Koopman transport operators.

This result essentially owes to three separate intuitions throughout the derivation: first, in a dynamical average, the action of the evolution operator can be shifted at will between the observable and the density; second, a time-dependent average is turned into the more meaningful phase-space distribution by setting the initial condition to a delta function centered at any point; third, the first non-trivial order truncation of the expansion of a pushed-forward or pulled-back chaotic field in terms of eigenfunctions of the transport operators gives rise to observable-independent field profiles, and thus universality at an intermediate timescale of integration.

The theory is validated on two-dimensional models of chaos, but its implications go as far as the applicability of the Koopman treatment to problems of fluid dynamics (e.g. passive scalars³², chaotic mixing³³, and turbulent aerosols³⁴), neuronal networks, weather science, and time-series analysis in general, while it may serve as a valuable complement for those interested in Lagrangian coherent structures^{22,35}, almost-invariant sets³⁶, or convective modes^{37,38}.

As conveyed by the numerical tests on the Hamiltonian Hénon map, the theory presented here may not necessarily be restricted to hyperbolic systems, but rather extend to (noisy) mixed dynamics, when concerned with timescales that only involve the discrete part of the transport operator spectrum.

On the other hand, the present treatment is limited to *i*) systems whose densities and fields are Lebesgue integrable at all times, unlike for example noiseless strange attractors, and *ii*) featuring a real-valued second eigenvalue and eigenfunction for the transport operators. If, instead, the second eigenvalue is a complex conjugate pair, decay of correlations and convergence to the (conditionally) invariant densities are not monotonic but oscillatory, and one can show that the field profile stemming from the leading nontrivial terms in the expansions (7) and (8) gets to depend on the choice of the observable, when the latter is real valued. This phenomenology is addressed in detail by a separate report²⁴.

Appendix A: Expansion truncations and timescales

In this section, I discuss the validity of the first-order truncation of the eigenfunction expansion in the expressions of

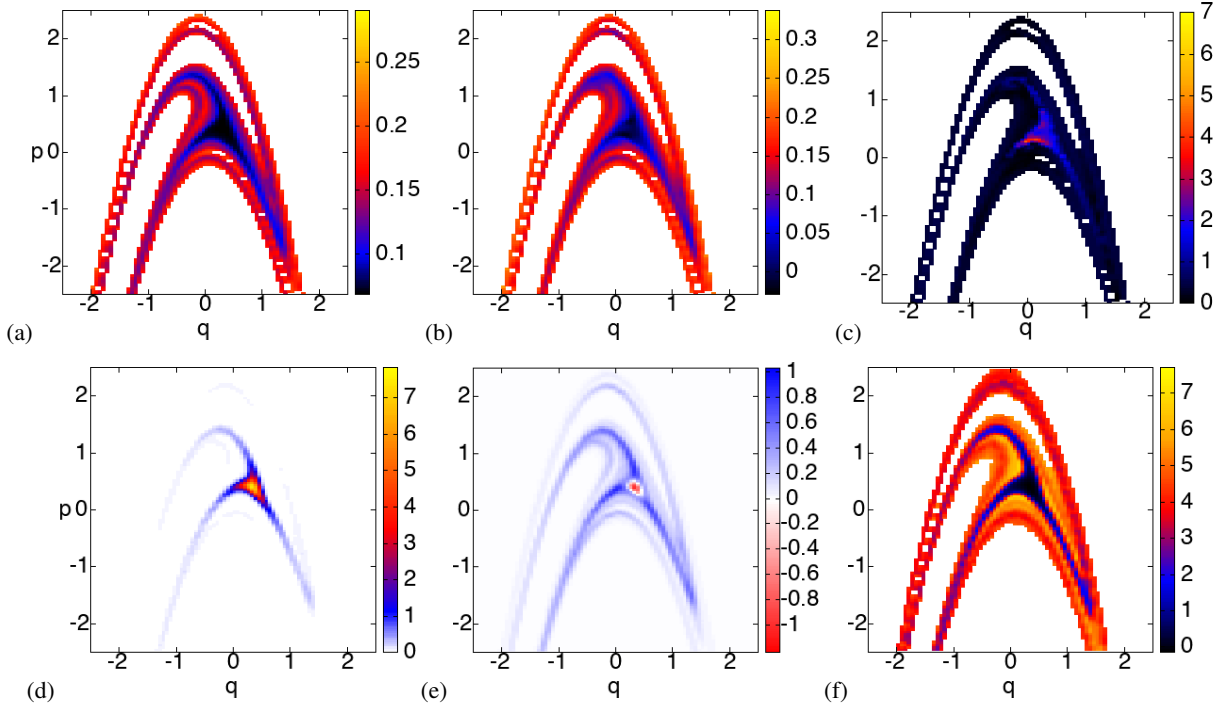


FIG. 4. Phase-space density plots (2^{14} points, each averaged over 10^4 trajectories) of integrated observables of the Hénon map with white, Gaussian noise of amplitude $\Delta = 10^{-3}$, pinned by the initial points, after $t = 10$ iterations of the map: (a) diffusivity; (b) finite-time Lyapunov exponents; (c) ratio of (a) to (b), as defined in (22). (d) The leading eigenfunction of the Koopman operator for the same noisy map, approximated with the Ulam method on a matrix of size $2^{14} \times 2^{14}$; (e) the first subleading eigenfunction of the same matrix; (f) the ratio (in absolute value) of (e) to (d).

both instantaneous and integrated observables.

Let us begin with the instantaneous observables of Eqs. (7) (pushed forward) and (8) (pulled back): the expansion of the field may be continued, to include the next order, that is

$$\begin{aligned} \hat{a}^t(x_0) &\simeq \int_{\mathcal{M}} a(x) \phi_0(x) dx + \frac{\varphi_1(x_0)}{\varphi_0(x_0)} e^{-(\gamma_1 - \gamma_0)t} \int_{\mathcal{M}} a(x) \phi_1(x) dx \\ &+ \frac{\varphi_2(x_0)}{\varphi_0(x_0)} e^{-(\gamma_2 - \gamma_0)t} \int_{\mathcal{M}} a(x) \phi_2(x) dx, \end{aligned} \quad (\text{A1})$$

so that the relative magnitude of the second and third terms may be assessed by looking at their respective time-dependent prefactors

$$c_i(t) = e^{-(\gamma_i - \gamma_0)t} \int_{\mathcal{M}} a(x) \phi_i(x) dx. \quad (\text{A2})$$

Fig. 6 shows the decay of both $c_1(t)$ and $c_2(t)$ in the simulations of the perturbed cat map and the observable $a(x) = q^2(x)$, where the first term consistently exceeds the second by at least two orders of magnitudes over the time scale of relaxation of the system to statistical equilibrium, determined by the spectral gap (figures of the same order were found for the other observables considered in this work). It is noted that the second and third eigenfunctions $\varphi_1(x)$ and $\varphi_2(x)$ take values of the same order, both being L_1 -normalized. Besides the fact that $\gamma_2 > \gamma_1$, higher-order eigenfunctions tend to increasingly oscillate^{39,40}, and thus the integral $\int_{\mathcal{M}} a(x) \phi_i(x) dx$ decreases in absolute value, as i

grows. As a consequence, the third eigenvalue $e^{-\gamma_2}$ of the transfer operator need not be much smaller than the second $e^{-\gamma_1}$ (in this calculation they only differ by 4%) in order for the truncation to the second term in the expansion to closely approximate $\hat{a}^t(x_0)$ for much of the relaxation time to equilibrium or stationarity. On the other hand, the first non-trivial contribution to the expansion (A1), which in the cat map is found to be $O(10^{-1})$ at intermediate times for the all the observables studied, is significant with respect to the leading term, that is of the order of unity.

Next, let us examine integrated observables. Here the analysis is slightly more involved, since the factors $\int_{\mathcal{M}} A^t(x) \phi_1(x) dx$ in the expansion

$$\begin{aligned} \hat{A}^t(x_0) &\simeq \int_{\mathcal{M}} A^t(x) \phi_0(x) dx + \frac{\varphi_1(x_0)}{\varphi_0(x_0)} e^{-(\gamma_1 - \gamma_0)t} \int_{\mathcal{M}} A^t(x) \phi_1(x) dx \\ &+ \frac{\varphi_2(x_0)}{\varphi_0(x_0)} e^{-(\gamma_2 - \gamma_0)t} \int_{\mathcal{M}} A^t(x) \phi_2(x) dx, \end{aligned} \quad (\text{A3})$$

are time dependent. If our observable is of the form $a(x) = g(x)$, that is a function of the coordinates (like diffusivity and kinetic energy, unlike the Lyapunov exponent), however, it is possible to go back to the definition (9) of integrated observable, rewrite it in terms of the Koopman operator, as

$$A^t(x) = \int_0^t a[f^\tau(x)] d\tau = \int_0^t \mathcal{L}_\tau^\dagger a(x) d\tau,$$

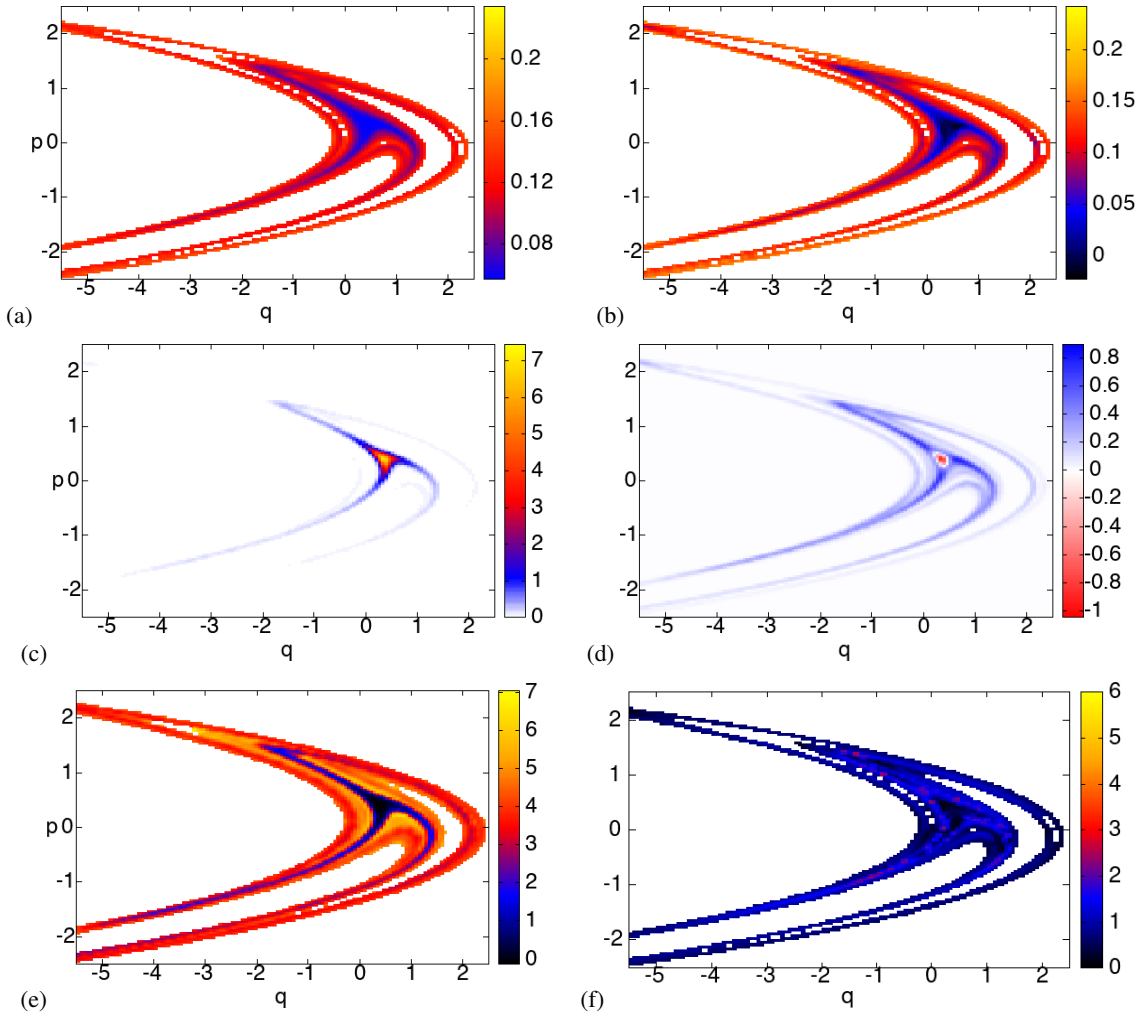


FIG. 5. Phase-space density plots (2^{14} points, each averaged over 10^4 trajectories) of integrated observables of the Hénon map with white, Gaussian noise of amplitude $\Delta = 10^{-3}$, pinned by the final points, after $t = 10$ iterations of the map: (a) diffusivity; (b) finite-time Lyapunov exponents. (c) The leading eigenfunction of the Perron-Frobenius operator for the same noisy map, approximated with the Ulam method on a matrix of size $2^{14} \times 2^{14}$; (d) the first subleading eigenfunction of the same matrix; (e) the ratio (in absolute value) of (d) to (c). (f) Ratio of (a) to (b), as defined in (22).

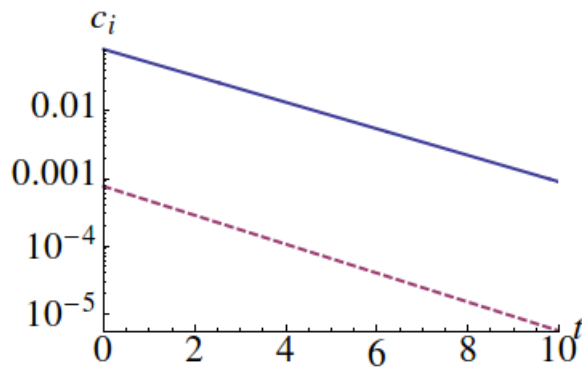


FIG. 6. (Log-scale) The prefactors $c_1(t)$ (solid line) and $c_2(t)$ (dashed line) as defined in Eq. (A2), computed for the perturbed cat map model and the observable q^2 , versus time.

and expand $\mathcal{L}_\tau^\dagger a(x)$ in terms of the eigenspectrum of \mathcal{L}_τ^\dagger . That way, every factor multiplying the eigenfunction ratio $\varphi_i(x_0)/\varphi_0(x_0)$ in Eq. (A3) is written as

$$\begin{aligned} c_i(t) &= e^{-(\gamma_i - \gamma_0)t} \sum_j \hat{b}_j \frac{1 - e^{-\gamma_j t}}{\gamma_j} \int_{\mathcal{M}} \varphi_j(x) \varphi_i(x) dx \\ &= \hat{b}_i e^{-(\gamma_i - \gamma_0)t} \frac{1 - e^{-\gamma_i t}}{\gamma_i}, \end{aligned} \quad (\text{A4})$$

for the bi-orthonormality of the eigenfunctions of \mathcal{L}^\dagger and \mathcal{L} , with $\hat{b}_i = \int_{\mathcal{M}} \varphi_i(x) a(x) dx$. It is immediately apparent the difference of the time-dependent part of $c_i(t)$ here in comparison with Eq. (A2) for an instantaneous observable. Fig. 7(a) illustrates this behavior, and in particular it features a slower relaxation to equilibrium for an integrated observable than for an instantaneous one. That explains why the phase-space profiles of $A^t(x)$ still bear signatures of the second eigenfunction for a relatively large value of t in the snapshots of

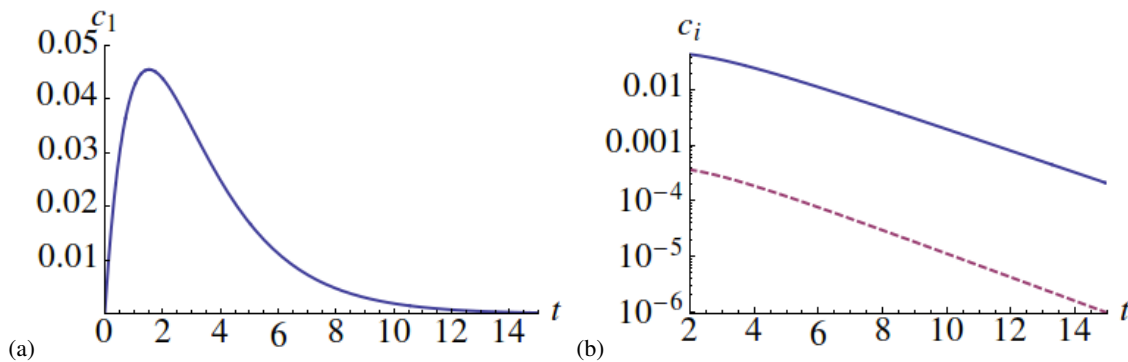


FIG. 7. (a) The prefactor $c_1(t)$, as defined in Eq. (A4), computed for the perturbed cat map model and the integrated observable $A^t(x) = \int_0^t d\tau q^2(f^\tau(x))$, versus time. (b) (Log-scale) The decay of the prefactors $c_1(t)$ (solid line) and $c_2(t)$ (dashed line) versus time, for the same system and integrated observable.

Figs. 2, 3, 4, 5. Like in the case of an instantaneous observable, I now compare the prefactors c_1 and c_2 of the second and third eigenfunctions respectively, this time given by Eq. (A4), in the example of the perturbed cat map, for the observable $A^t(x) = \int_0^t d\tau q^2(f^\tau(x))$. The outcome (Fig. 7(b)) confirms the conclusions drawn for instantaneous observables, where the coefficient of the third term in the expansion is consistently at least two orders of magnitudes smaller than that of the second at an intermediate time scale toward relaxation, and thus justifies the truncation that motivates the fields universal behavior claimed here. The contribution of the factor $\hat{b}_i = \int_{\mathcal{M}} \phi_i(x) a(x) dx$ is again decisive, and so is the increasingly oscillatory behavior of $\phi_i(x)$ with the order i of the eigenfunction.

- ¹O. Bratteli and P. Jorgensen, *The Transfer Operator and Perron-Frobenius Theory* (Birkäuser, Basel, 2002).
- ²P. Cvitanović, R. Artuso, R. Mainieri, G. Tanner, and G. Vattay, *Chaos: Classical and Quantum* (Niels Bohr Institute, Copenhagen, 2020).
- ³R. Mohr and I. Mezić, “Applied Koopmanism,” *Chaos* **22**, 047510 (2012).
- ⁴M. L. Kringelbach and G. Deco, “Brain states and transitions: Insights from computational neuroscience,” *Cell Reports* **32**, 108128 (2020).
- ⁵R. M. D’Souza, M. di Bernardo, and Y.-Y. Liu, “Controlling complex networks with complex nodes,” *Nature Reviews Physics* **5**, 250 (2023).
- ⁶L. Alonso, J. A. Méndez-Bermúdez, A. González-Meléndrez, and Y. Moreno, “Weighted random-geometric and random-rectangular graphs: spectral and eigenfunction properties of the adjacency matrix,” *Journal of Complex Networks* **6**, 753 (2018).
- ⁷C. Zhang, H. Li, and Y. Lan, “Phase space partition with Koopman analysis,” *Chaos* **32**, 063132 (2022).
- ⁸S. C. Kapfer and W. Krauth, “Irreversible local Markov chains with rapid convergence towards equilibrium,” *Physical Review Letters* **119**, 240603 (2017).
- ⁹S. Klus, F. Nüske, S. Peitz, J.-H. Niemann, C. Clementi, and C. Schütte, “Data-driven approximation of the Koopman generator: Model reduction, system identification, and control,” *Physica D* **406**, 132416 (2020).
- ¹⁰C. C. Maiocchi, V. Lucarini, and A. Gritsun, “Decomposing the dynamics of the Lorenz 1963 model using unstable periodic orbits: Averages, transitions, and quasi-invariant sets,” *Chaos* **32**, 033129 (2022).
- ¹¹A. N. Souza, “Transforming butterflies into graphs: Statistics of chaotic and turbulent systems,” arXiv.2304.03362 (2023).
- ¹²J. Slipantschuk, O. F. Bandtlow, and W. Just, “On the relation between lyapunov exponents and exponential decay of correlations on the relation between lyapunov exponents and exponential decay of correlations,” *Journal of Physics A: Mathematical and Theoretical* **46**, 075101 (2013).
- ¹³G. Froyland, “On Ulam approximation of the isolated spectrum and eigen-

- functions of hyperbolic maps,” *Discrete & Continuous Dynamical Systems* **17**, 671 (2007).
- ¹⁴K. Yoshida, H. Yoshino, A. Shudo, and D. Lippolis, “Eigenfunctions of the Perron-Frobenius operator and the finite-time Lyapunov exponents in uniformly hyperbolic area-preserving maps,” *Journal of Physics A: Mathematical and Theoretical* **54**, 285701 (2021).
- ¹⁵D. Lippolis, A. Shudo, K. Yoshida, and H. Yoshino, “Scarring in classical chaotic dynamics with noise,” *Physical Review E* **103**, L050202 (2021).
- ¹⁶E. M. Bollt and S. D. Ross, “Is the finite-time Lyapunov exponent field a Koopman eigenfunction?” *Mathematics* **9**, 2731 (2021).
- ¹⁷In what follows, the word distribution is understood as phase-space function, say $a(x)$, and not as probability density function.
- ¹⁸M. Blank, G. Keller, and C. Liverani, “Ruelle-Perron-Frobenius spectrum for Anosov maps,” *Nonlinearity* **15**, 1905 (2002).
- ¹⁹P. Gaspard, *Chaos, Scattering, and Statistical Mechanics* (Cambridge University Press, Cambridge, 1999).
- ²⁰E. Altmann, J. S. E. Portela, and T. Tél, “Leaking chaotic systems,” *Reviews of Modern Physics* **85**, 869 (2013).
- ²¹G. Froyland, “An analytic framework for identifying finite-time coherent sets in time-dependent dynamical systems,” *Physica D*, 1 (2013).
- ²²H. Aref *et al.*, “Frontiers of chaotic advection,” *Reviews of Modern Physics* **89**, 025007 (2017).
- ²³Z. Ahsan, H. Dankowicz, and C. Kuehn, “Adjoint-based projections for uncertainty quantification near stochastically perturbed limit cycles and tori,” arXiv.2404.13429 (2024).
- ²⁴D. Lippolis, “Thermodynamics of chaotic relaxation processes,” arXiv.2404.09130 (2024).
- ²⁵H. Risken, *The Fokker-Planck Equation* (Springer, Berlin, 1996).
- ²⁶P. Cvitanović and D. Lippolis, “Knowing when to stop: how noise frees us from determinism,” *AIP Conference Proceedings* **1468**, 82 (2012).
- ²⁷S. M. Ulam, *A Collection of Mathematical Problems* (Interscience, New York, 1960).
- ²⁸T.-Y. Li, “Finite approximation for the Perron-Frobenius operator, a solution to Ulam’s conjecture,” *Journal of Approximation Theory* **17**, 177 (1976).
- ²⁹D. J. Chappell, M. Richter, G. Tanner, O. F. Bandtlow, W. Just, and J. Slipantschuk, “Ray-tracing the Ulam way,” in *Integral Methods in Science and Engineering*, edited by C. Constanda, B. E. J. Bodmann, and P. J. Harris (Birkhäuser, 2023) Chap. 8.
- ³⁰L. Ermann and D. L. Shepelyansky, “The Arnold cat map, the Ulam method, and time reversal,” *Physica D* **241**, 514 (2012).
- ³¹V. I. Arnold and A. Avez, *Ergodic Problems of Classical Mechanics* (Benjamin, New York, 1968).
- ³²Z. Warhaft, “Passive scalars in turbulent flows,” *Annual Review of Fluid Mechanics* **32**, 203 (2000).
- ³³J.-L. Thiffeault, “Scalar decay in chaotic mixing,” *Lecture Notes in Physics* **744**, 3 (2007).
- ³⁴J. Bec, K. Gustavsson, and B. Mehlig, “Statistical models for the dynamics of heavy particles in turbulence,” *Annual Review of Fluid Mechanics* **56**,

- 189 (2024).
- ³⁵G. Haller, “Lagrangian coherent structures,” *Annual Review of Fluid Mechanics* **47**, 137 (2015).
- ³⁶G. Froyland, “Unwrapping eigenfunctions to discover the geometry of almost-invariant sets in hyperbolic maps,” *Physica D* **237**, 840 (2008).
- ³⁷C. Blachut and S. Balasuriya, “Convective modes reveal the incoherence of the Southern Polar Vortex,” *Scientific Reports* **14**, 966 (2024).
- ³⁸G. Froyland, D. Giannakis, B. R. Lintner, M. Pike, and J. Slawinska, “Spectral analysis of climate dynamics with operator-theoretic approaches,” *Nature Communications* **12**, 6570 (2021).
- ³⁹H. H. Hasegawa and D. J. Driebe, “Intrinsic irreversibility and the validity of the kinetic description of chaotic systems,” *Physical Review E* **50**, 1781 (1994).
- ⁴⁰H. H. Hasegawa, D. J. Driebe, and C.-B. Li, “Spectral decomposition of the stretching dynamics of the Arnold cat map,” *Physics Letters A* **319**, 290 (2003).